The prediction of mechanical performance of isotactic polypropylene on the basis of processing conditions

Polymer 83 (2016) 116–128

Contents lists available at ScienceDirect

Polymer

journal homepage: www.elsevier.com/locate/polymer

The prediction of mechanical performance of isotactic polypropylene on the basis of processing conditions

H.J.M. Caelers, L.E. Govaert, G.W.M. Peters*

Department of Mechanical Engineering, Materials Technology Institute, Eindhoven University of Technology, P.O.Box 513, 5600 MB, Eindhoven, The Netherlands

ARTICLE INFO

Article history:
Received 30 September 2015
Received in revised form
30 November 2015
Accepted 1 December 2015
Available online 18 December 2015

Keywords:
Semi-crystalline polymer
Structure-property relations
Lamellar thickness
Yield stress

ABSTRACT

A strategy is presented to predict the yield kinetics following from different thermomechanical histories experienced during processing in non-isothermal quiescent conditions. This strategy deals with three main parts, i.e. processing, structure and properties. In the first part the applied cooling conditions are combined with the crystallization kinetics and the cooling history of the material is calculated. From this history the lamellar thickness distributions are predicted in the second part. Finally, in the third part these distributions are used to predict yield stresses. Experimental validation is carried out for all the different parts of the strategy. In situ temperature measurements, lamellar thickness distributions from SAXS experiments and yield stresses measured in uniaxial tensile deformation are performed for validation purposes. The versatility is investigated by applying this procedure on two different iPP grades. The yield stress predictions show good agreement with the experimentally obtained results in two separate deformation mechanisms, and only a few parameters are dependent on the specific iPP grades that were used here. Moreover, it is shown that the average lamellar thickness is sufficient to predict the yield stress, and that the width of lamellar thickness distributions does not have to be taken into account.

1. Introduction

Polymers are used in a wide spectrum of applications ranging from packaging to structural engineering. Polyolefins, specifically polyethylene and polypropylene, form a substantial part of the synthetic polymers used because of their low costs, ease of manufacturing and versatility. To illustrate, these materials are used in extrusion processes (pipes), film blowing processes (packaging) and injection molding processes (structural applications). Within this specific class of materials multiple variants of polypropylene exist, e.g. isotactic-, syndiotactic-, atactic polypropylene and many copolymers. Their properties are related to the chemical structure, in particular the presence of regularity [1], since it allows polypropylene (iPP and sPP) to partially crystallize upon cooling. Due to the ability to crystallize the solidification takes place at higher temperatures as compared to aPP, largely affecting the mechanical properties. Other important aspects dominating the morphology and thereby the mechanical properties, are the processing conditions. Flow and cooling conditions are known to largely affect the morphology and therewith the yield kinetics and overall mechanical response [2,3]. Since changes of these processing conditions throughout a product may therefore result in strong spatial variations of mechanical performance [4], an undesired consequence is that weak spots are typically present. In this work a first attempt is made to relate the mechanical properties to the morphology resulting from well-defined processing conditions.

The solid crystalline parts, present in iPP, are connected by chains surpassing the amorphous regions [5,6]. Some general findings on the relation between the crystals and the mechanical properties follow from several studies performed in the past. First, the Young's modulus increases with the degree of crystallinity, whereas the impact performance and the toughness decrease [7,8]. Furthermore, the yield stress appears to be strongly correlated to lamellar thickness [9–14]. This relation was rationally based on the nucleation and propagation of screw dislocations [12] in the crystalline lamellae and thus on the lamellar thickness.

Besides the variations in the thickness of the crystalline domains (lamellae), multiple crystallographic structures can be present. In iPP, monoclinic α, pseudo-hexagonal β, orthorhombic γ and mesomorphic unit cell structures [15,16] can be formed with alternating amorphous and rigid amorphous regions in between

* Corresponding author.
E-mail address: g.w.m.peters@tue.nl (G.W.M. Peters).

http://dx.doi.org/10.1016/j.polymer.2015.12.001
0032-3861/

[17], affecting the mechanical properties as well. The presence of these regions together with the polymorphism makes it complicated to reveal the relationship between mechanical properties observed on a macroscopic scale to morphologies present at a microscopic or even smaller nanometer scale [18].

The crystallization process is kinetically controlled and therefore local thermo-mechanical conditions experienced by the polymer during processing can have pronounced effects on the lamellar morphology that forms, as well as on the polymorphism within the crystals [19–21,4]. Structure development under processing conditions has been subject of substantial research carried out in the past [22–24]. When we focus on conditions imposed during a compression molding process, i.e. moderate non-isothermal quiescent conditions, it is found that in the case of neat iPP typically α crystals develop [25]. Depending on the applied cooling rate, the crystallinity as well as the number and size of spherulites varies. Furthermore, this unavoidably results in variations of the lateral size of the crystal sheet-like domains, but more important for the yield kinetics, differences in the thickness will appear. The lamellar thickness is determined by the undercooling during the crystallization process [26] and, therefore, directly related to the cooling rate. Van Erp et al. [3] specified this effect of cooling rate to investigate the structure property relation for iPP. On the other hand, several studies have been devoted to the development of model frameworks capable of quantitatively predicting the processing dependent crystal structures as a result of processing [25,27–30].

The main aim of this work was to make a coupling between the processing-structure and structure-property relation in a predictive way. The strategy chosen to accomplish this goal is schematically shown in Fig. 1 and is divided into three main blocks. Different processing histories are obtained in terms of variable cooling rates. In the first block the processing dependent crystallization kinetics are predicted as a function of time and temperature. The time-temperature history follows from the heat equation, which is used in combination with the crystallization model proposed by van Drongelen et al. [25] to account for latent heat release. Temperature and pressure dependent growth rate and nucleation density are the most important parameters governing the crystallization process, whereas the boundary conditions together with the thermal contact resistance determine the temperature evolution. In the second block the obtained evolution of crystal volume as a function of temperature is used in combination with the Lauritzen-Hoffman equation [26] to determine the lamellar thickness distributions resulting from the different cooling rates. Also the dependency of the molecular properties of the iPP chain on the crystallization temperature and lamellar thickness is determined. Finally, in block three, the lamellar thickness is used to get the yield kinetics by making use of an empirical relation reported by van Erp et al. [3].

In the present study we will first give more detailed background information on 1) the crystallization model and the simplifications that are used, 2) the coupling to a structural feature, in this case lamellar thickness and 3) the relation between the lamellar thickness and the yield kinetics. Subsequently these three distinct parts are coupled and used to predict yield stresses resulting from well defined thermo-mechanical histories. The validity of this approach is experimentally shown for two iPP grades.

2. Experimental

2.1. Materials

Two isotactic polypropylene homopolymer grades were used: iPP-1 (Borealis HD234CF) with a weight averaged molar weight Mw = 310 kg/mol and a polydispersity Mw/Mn = 3.4, and iPP-2 (Borealis HD601CF) with Mw = 365 kg/mol and Mw/Mn = 5.4. These two materials were chosen because they were used in several other crystallization studies in our group [25,31].

2.2. Sample preparation

To obtain samples with different thermal histories, sheet material with a thickness of 1 mm was compression molded from both the iPP-1 an iPP-2 grade. A mold, sample surface area of 100 cm^2, was sandwiched in between stainless steel sheets (0.5 mm) and placed in a hot press, see Fig. 2. The stack was subsequently heated to 230 °C and a force of 100 kN was applied stepwise. The sheets were kept under these conditions for 3 min to erase previous thermo-mechanical history. The solidification was induced by putting the stack in a cold press for 3 min, at temperatures varying from 20 °C to 90 °C (steps of 10 °C). To monitor the temperature

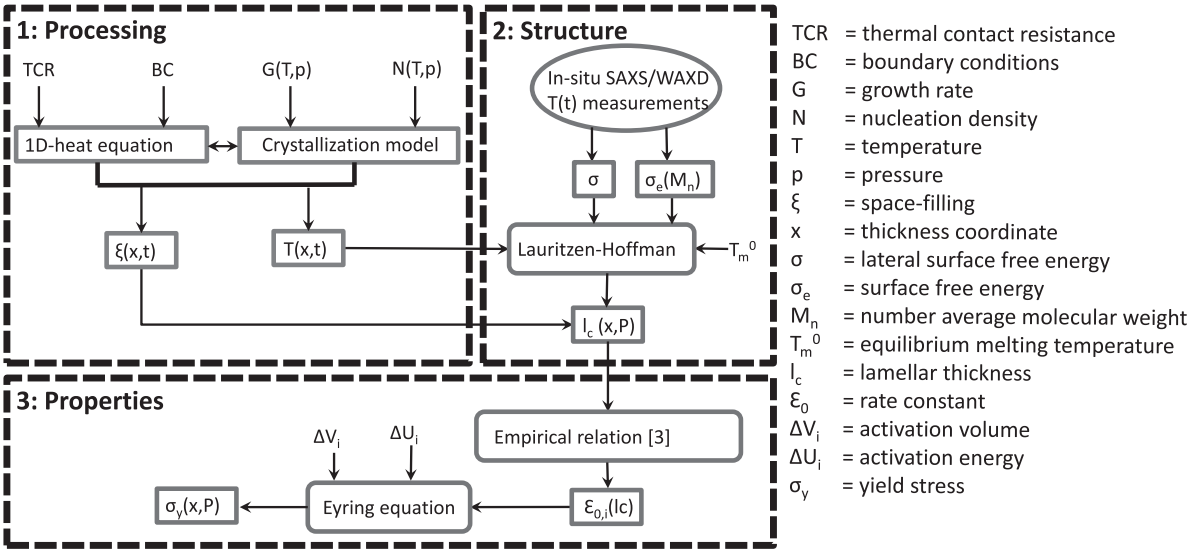

Fig. 1. Strategy to predict the yield stress directly from processing conditions.

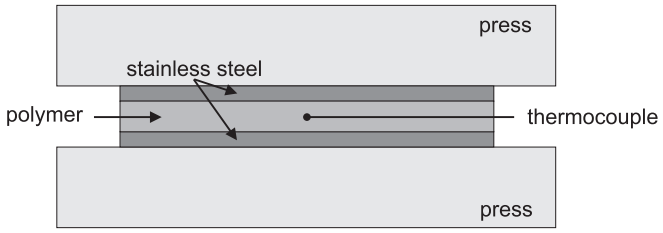

Fig. 2. Schematic representation of the compression molding process.

during solidification, a small calibrated thermocouple was embedded in the polymer. A fast acquisition datalogger (National Instruments Hi-speed USB 9162, sampling frequency 10 Hz) was used to record the temperature in-situ.

2.3. X-ray

Small angle X-ray scattering (SAXS) and wide angle X-ray diffraction (WAXD) experiments were performed at the Dutch-Belgian (DUBBLE) beamline BM26 [32] of the European Synchrotron and Radiation Facility (Grenoble, France). Quasi-isothermal crystallization experiments were performed with a custom modified JHT-350 Linkam stage equipped with a pneumatically actuated temperature jump-stage [33]. The cold stage was set at temperatures of 100, 110 and 120 °C respectively. To monitor the temperature and quasi-isothermal crystallization in time, a small thermocouple was embedded in the polymer. In-situ WAXD ans SAXS patterns were recorded with acquisition rates of 20 frames per second. A wavelength of $\lambda = 1.04$Å was used. The 2D SAXS patterns were recorded with a Pilatus 1 M detector and the WAXD patterns with a Pilatus 300 K detector, both with pixel size of 172×172 μm^2, placed at approximately 1.42 and 0.30 m respectively.

Single shots were obtained ex-situ from the compression molded samples with the different cooling histories, with an acquisition time of 10 s. All the acquired images were corrected for beam intensity and scattering of the empty sample cell.

3. WAXD

The obtained intensity profiles were plotted versus the scattering angle 2θ. The weight fraction of the crystallinity χ_w was determined with Eq. (1):

$$\chi_w = \frac{C_{tot} - C_a}{C_{tot}} \tag{1}$$

where C_{tot} is the total scattered intensity and C_a is the scattered intensity of an amorphous halo. The amorphous halo is measured on a quenched low tacticity polypropylene sample with negligible crystallinity, and scaled with the minimum between the $(110)_\alpha$ and $(040)_\alpha$ diffraction peaks [34]. The volume fraction of the crystallinity is given by Ref. [9]:

$$\chi = \frac{\frac{\chi_w}{\rho_c}}{\frac{\chi_w}{\rho_c} + \frac{1-\chi_w}{\rho_a}} \tag{2}$$

where ρ_a and ρ_c are the density of the amorphous and crystalline phase respectively, taken from Ref. [35].

4. SAXS

The scattered intensity was obtained as a function of the scattering vector q which is given by:

$$q = \frac{4\pi}{\lambda} sin(\theta) \tag{3}$$

where θ is half of the scattering angle. In case of an isotropic system with a randomly oriented lamellar morphology the measured scattering intensity can be transposed into the 1D scattering intensity using Lorentz correction:

$$I_1(q) = I(q)q^2 \tag{4}$$

Once this correction is performed and the electron density differences in one direction are known, the average lamellar thickness l_c can be obtained from:

$$l_c = \frac{2\pi}{q_{I_1,max}} \chi \tag{5}$$

where $q_{I_1,max}$ is the value for the magnitude of the scattering vector q, corresponding to the maximum of the Lorentz corrected scattering intensity, and χ is the crystalline volume fraction. This method provides an average lamellar thickness. Information about lamellar thickness distributions was obtained using the interface distribution function (IDF) which is the second derivative of the 1D-correlation function $\gamma_1(r)$ (Eq. (7)) [36,37], and is defined as:

$$g_1(r) = \frac{\delta^2\gamma(r)}{\delta r^2} = -\frac{1}{Q}\int_{q_0}^{q_\infty} I_1(q)q^2 cos(qr)\, dq \tag{6}$$

with

$$\gamma_1(r) = \frac{1}{Q}\int_{q_0}^{q_\infty} I_1(q) cos(qr)\, dq \tag{7}$$

where Q is the invariant and r is the real space. The interface distribution function $g_1(r)$ can also be obtained by taking the inverse Fourier transform of the interference function $G_1(q)$ [38]

$$g_1(r) = \int_{q_0}^{q_\infty} G_1(q) cos(qr)\, dq \tag{8}$$

in which

$$G_1(q) = \lim_{q\to\infty} I_1(q)q^2 - I_1(q)q^2. \tag{9}$$

Since the Fourier transform requires integration from $q = 0$ to infinite, the experimentally accessable q range has to be extrapolated. The triangle rule is used to extrapolate to zero q, whereas the Porod law is used to extrapolate to infinite q. In an ideal two-phase system with sharp boundaries the Porod law predicts a decay in scattered intensity proportional to q^{-4} at large angles. In reality the intensity often deviates from such an ideal system because of electron density fluctuations and finite interfaces between the crystalline and the amorphous layers. When taking these deviations into account, the adapted Porod law is given by Ref. [39]:

$$\lim_{q\to\infty} I_{obs}(q) = I_b(q) + \frac{K_p}{q^4} exp\left(-\sigma^2 q^2\right) \tag{10}$$

where σ is related to the interface thickness, K_p is the Porod constant and I_b the scattering resulting from electron density fluctuations. The determination of the parameters required to correct for

non-ideality is a sensitive process which can be rather difficult in case of a noisy signal. For this reason an approach proposed by Hsiao et al. [40] is used, where constraints are used to find the parameters required for the intensity corrections. This fit is based on two properties that have to be fulfilled by the interference function. First, the difference between the asymptote at large values of q, following from the Porod law, and the ideal scattered intensity should become zero. Moreover, as a second constraint, the interface distribution function should start from the origin and as a result the total area of $G_1(q)$ versus q should be zero. Minimization of Eq. (11), which is only valid in the porod region, and Eq. (12) gives the values for the Porod constant, the interface thickness and the liquid-like scattering.

$$\lim_{q\to\infty} G_1(q) = \lim_{q\to\infty}\left[K_p - [I_{obs}(q) - I_b(q)]q^4 exp\left(\sigma^2 q^2\right)\right] = 0 \quad (11)$$

$$\int_{q_0}^{q_\infty} G_1(q)\,\mathrm{d}q = \int_{q_0}^{q_\infty}\left[K_p - (I_{obs}(q) - I_b(q))q^4 exp\left(\sigma^2 q^2\right)\right]\mathrm{d}q = 0 \quad (12)$$

The background intensity following from the electron density fluctuation or liquid like scattering is expressed by

$$I_b(q) = a + bq^2 + cq^4 + dq^6 \quad (13)$$

The most reliable average value and the distribution of the lamellar thickness, the long spacing and the amorphous regions can be obtained by deconvolution of the interface distance distribution function $g_1(r)$. Long spacings obtained by Bragg's law are typically considerably larger then the true values, especially when distributions are broad [41]. This will irrefutable result in erroneous lamellar thicknesses found with the method of combining WAXD and SAXS measurements Eq. (5).

4.1. Mechanical testing

A punch was used to cut typical dog-bone shaped tensile test samples (according to ASTM D1708) from the different compression molded polymer sheets. A Zwick Z010 universal tensile tester equipped with a 2.5 kN load cell and a thermostatically controlled oven was used to perform the tensile tests at strain rates of 10^{-3} s^{-1}. The tests were performed at 23 °C and 80 °C. In advance of the measurements at elevated temperatures, the tensile specimen was kept at the test temperature for 5 min (which is sufficient to achieve thermal equilibrium) before a pre-load of 0.2 MPa was applied. All tests were carried out at least in duplicate. Tensile tests were performed immediately after sample preparation to avoid effects of aging at room temperature [42–44].

5. Background

5.1. Thermal analysis

Cooling rate affects the crystallization process of iPP, but conversely, the cooling rate is influenced by the crystallization process because latent heat releases. This mutual influence of the cooling and crystallization process is elaborated in terms of a 1D conduction problem. In al the experimental test cases performed in this work the polymer layer is positioned in between layers of stainless steel. These are included in the model in order to get the boundary conditions right.

5.1.1. The heat balance

To predict the temperature profile in the polymer, the 1D heat equation for conduction is used:

$$\rho(P,\xi,T)\cdot C_p(\xi,T)\cdot\frac{\partial T}{\partial t} = \frac{\partial}{\partial x}\left(\lambda(\xi,T)\cdot\frac{\partial T}{\partial x}\right) + \rho(P,\xi,T)\cdot\Delta H\cdot\dot{\xi} \quad (14)$$

In this equation the specific heat C_p [J/kg K], the density ρ [kg/m^3] and the thermal conductivity λ [W/mK] are all functions of temperature and crystallinity. The effect of pressure on the density is not taken into account. The last term of Eq. (14) is the source term, representing the latent heat release due to crystallization [45]. The time derivative of the space filling, $\dot{\xi}$, follows directly from the crystallization model described in Section 5.2 and ΔH [J/kg] is the total enthalpy of transformation. To capture the phase dependent thermal properties a simple mixing rule, Eq. (15), is used which is similar for heat capacity, density and thermal conductivity.

$$C_p(\xi,T) = \xi C_{p_{sc}}(T) + (1-\xi)C_{p_a}(T) \quad (15)$$

The heat capacity and the thermal conductivity are linearly proportional to the temperature, whereas the density is proportional to the reciprocal temperature [35]. Subscripts a and sc refer to the amorphous and semi-crystalline phase, respectively. Heat transfer in the aluminum and steel layers of the experimental setup is again described with the 1D heat equation. However, in that case the thermal properties are assumed to be constant and the source term disappears. Therefore Eq. (14) reduces to:

$$\rho C_p\frac{\partial T}{\partial t} = \lambda\left(\frac{\partial^2 T}{\partial x^2}\right) \quad (16)$$

The parameters that were used in the heat equation are given in Table 1.

5.1.2. Thermal contact resistance

The experimental setup consists of a stack of polymer-, and stainless steel layers. As a result of surface roughness or interstitial materials, a pressure dependent thermal contact resistance is present between the layers. Moreover, the state of the polymer, melt or solid, influences the thermal contact behavior.

This contact behavior is included in the model using Eq. (17). No data is available on pressure and state dependency, so the thermal contact resistance is assumed to be constant. It follows that the heat flux through the interface is given by:

$$\varphi_{int}(t) = \frac{T_{surf1} - T_{surf2}}{TCR} \quad (17)$$

where $\varphi_{int}(t)$ [W/m^2] is the heat flux from surface T_{surf1} [K] to surface T_{surf2} [K], and TCR [m^2 K/W] the thermal contact resistance. The ingoing heat flux (conduction) equals the flux through the interface, and the outgoing heat flux:

$$\varphi_{in}(t) = \varphi_{int}(t) = \varphi_{out}(t) \quad (18)$$

This results in:

Table 1
List of constants.

	ρ [kg/m^3]	Cp [J/kg K]	λ [W/mK]
Stainless steel	7930	502	17

$$\lambda_A \frac{dT}{dx}\bigg|_{left} = \varphi_{int}(t) = \lambda_B \frac{dT}{dx}\bigg|_{right} \tag{19}$$

were λ_A and λ_B are the thermal conductivities that belong to material A and B respectively. This is approximated by using the temperature gradient over the neighboring grid points:

$$\lambda_A \frac{\Delta T}{\Delta x}\bigg|_{left} = \frac{T_{surf1} - T_{surf2}}{TCR} = \lambda_B \frac{\Delta T}{\Delta x}\bigg|_{right} \tag{20}$$

After discretization using a finite difference method, the heat equation is solved using an implicit Euler scheme. The thermal contact resistance is determined by using the initial slope of the cooling curve for the fastest cooling rate. The parameter values used in the model for the thermal contact resistance are given in Table 2. For both iPP grades the same temperature dependent relations for density, specific heat and thermal conductivity are used [35] which explains why the fitted thermal contact resistance between the polymer and the stainless steel is different.

5.2. Crystallization kinetics

Crystallization of iPP is influenced by the chain architecture. Isotacticity is a key parameter with significant effects on crystallinity, polymorphism [46] and crystallization temperature [47]. Molecular weight affects the crystallization temperature [48]. Besides these chain architectural features the thermomechanical history experienced during processing is of significant importance. In the absence of flow and shear, the arising morphology and the crystallographic structures present therein are determined by the cooling rate [49] and pressure [19]. In this work we focus on the relationship between processing and structure, which has been subject to substantial research, and is captured in multiple crystallization models, many of them lacking structural details. A validated model to describe the temperature and pressure dependent crystallization behavior of iPP in detail, i.e. local nucleation density, spherulite size etc., was proposed by van Drongelen et al. [25]. This model framework is capable of predicting multiphase structure development in quiescent non-isothermal isobaric conditions. In this work a simplified version of this model is used which only allows monoclinic alpha phase formation. From WAXD measurements it is shown later that the model is applicable for the thermomechanical histories assessed in this study.

5.2.1. The crystallization model

Crystallization is dominated by nucleation and growth. In quiescent conditions the nuclei grow radially until they finally impinge and reach complete space filling. This can be described with the Kolmogoroff equation [50], which gives the space filling as a result of nucleation and growth in an unconfined 3-dimensional space according to:

$$\xi(t) = \frac{\chi(t)}{\chi_\infty} = 1 - exp(-\phi_0(t)) \tag{21}$$

where $\chi(t)$ is the crystallized volume fraction at time t and χ_∞ is the crystallinity when equilibrium is reached. The expected crystallized volume fraction if no impingement would occur $\phi_0(t)$ is given by Ref. [50]:

$$\phi_0(t) = \frac{4\pi}{3} \int_{-\infty}^{t} dt' \alpha(t') \left[\int_{-\infty}^{t} du G(u) \right]^3 \tag{22}$$

In this equation $\alpha(t) = \alpha(T(t), p(t))$ and $G(u) = G(T(u), p(u))$ are the (spherulitical) nucleation and growth rate respectively, both functions of temperature and pressure. In the special case of isothermal isobaric crystallization where growth rate and nucleation density (i.e. heterogeneous nucleation) are constants, the space filling in time $\xi(t)$ reduces to

$$\xi(t) = 1 - exp\left(-\frac{4\pi}{3} N G^3 t^3 \right) \tag{23}$$

which is known as the classical Avrami equation [51,52]. However, in this work non-isothermal crystallization is considered. Therefore, we start from the Kolmogoroff Eq. (22). To solve non-isothermal crystallization problems it is much easier to work with the Schneider rate equations which are basically a transform of this integral into a more suitable configuration. Now, $\phi_0(t)$ follows from the rate equations [53]:

$$\begin{aligned} \dot{\phi}_3 &= 8\pi \dot{N} \quad (\phi_3 = 8\pi N) \\ \dot{\phi}_2 &= G\phi_3 \quad (\phi_2 = 8\pi R_{tot}) \\ \dot{\phi}_1 &= G\phi_2 \quad (\phi_1 = S_{tot}) \\ \dot{\phi}_0 &= G\phi_1 \quad (\phi_0 = V_{tot}) \end{aligned} \tag{24}$$

where N is the number of nuclei (heterogeneous nucleation density), $\dot{N}$ is the nucleation rate, G is the spheruletic growth rate, R_{tot} is the sum of the spherulite radii, S_{tot} is the total surface of the spherulites and their total volume is given by V_{tot}. These structural features can be obtained since the nucleation and growth calculated via these equations, depend on the thermal history. The solution of these equations in isothermal conditions, and with a constant nucleation and growth rate, again results in Eq. (23). In this work the number of nuclei and the growth rate are temperature and pressure dependent and described by the expressions (25) and (26) respectively,

$$N(T,p) = N_{ref} exp\Big(-c_n \Big(T(t) - T_{Nref}(p) \Big) \Big) \tag{25}$$

$$G(T,p) = G_{max}(p) exp\Big(-c_g \Big(T(t) - T_{Gref}(p) \Big)^2 \Big) \tag{26}$$

where N_{ref} is the reference number of nuclei at the reference temperature T_{Nref}. G_{max} is the maximum growth rate at the reference temperature T_{Gref}, p is the pressure and c_n and c_g are constants. The effect of pressure on the nucleation density in incorporated by a shift in the reference temperature, and for the growth rate a shift of the reference temperature and a change in the maximum growth rate parameter G_{max} is included, according to the following equations,

$$T_{k,ref} = T^0_{k,ref} + \zeta (p - p_0) \cdot 10^{-5} \tag{27}$$

$$G_{max} = G^0_{max} exp\Big(a(p - p_0) + b(p - p_0)^2 \Big) \tag{28}$$

where $T^0_{k,ref}$ and G^0_{max} are the reference temperature and growth rate at atmospheric pressure p_0 in bar, and a, b and ζ are constants. The index k represents the growth (G) and nucleation (N).

Table 2
List of parameter values.

TCR in [m^2 K/W]	Press iPP-1	Press iPP-2
Stainless steel – stainless steel	$3 \cdot 10^{-4}$	$3 \cdot 10^{-4}$
Stainless steel – polymer	$4.1 \cdot 10^{-4}$	$6 \cdot 10^{-4}$

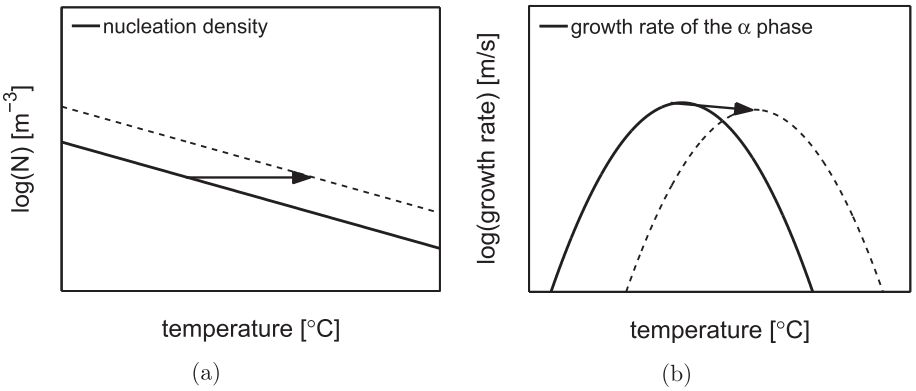

Fig. 3. a) Shift in the nucleation density as a result of pressure, b) Shift of the growth rate as a result of pressure. Adopted from Ref. [25].

In Fig. 3 it is schematically shown how the effect of pressure shifts the nucleation density and the growth rate respectively.

Finally, when the nucleation density and the growth rate are adapted for the applied pressure and non-isothermal conditions, the space filling in time $\dot{\xi}$ follows from:

$$\dot{\xi} = (1-\xi)\dot{\phi}_0 \tag{29}$$

An explicit Euler scheme is used to solve the crystallization model. The parameters required to describe the crystallization process are adopted from the work of van Drongelen et al. [25]. An overview is given in Table 3.

5.3. Deformation kinetics

5.3.1. Yield kinetics

To predict yield stresses resulting from well defined processing conditions we first look at the phenomena related to deformation kinetics. The behavior typically displayed by isotactic polypropylene is shown in Fig. 4(a). At low strains the stress increases linearly. With further increasing strain, the stress and the molecular mobility within the polymer increase as well. Ultimately, in the yield point, the molecular mobility is so high that the material deforms plastically at a rate equal to the applied strain rate. The stress associated with this point is defined as the maximum in the stress-strain response and called the yield stress. With increasing strain-rates higher molecular mobility is required for yielding. This is achieved by a higher stress level, explaining the rate dependency of the yield stress typically observed for polymers. Another way to induce mobility is raising the temperature. In the mechanical response this leads to decreasing yield stresses. After yielding strain softening takes place, leading to strain localization and subsequently necking.

The yield kinetics, i.e. the yield stresses over a broad range of temperatures and strain rates are shown in Fig. 4(b). From this figure it can directly be observed that the rate dependency at 23 °C is stronger then at 110 °C At an intermediate temperature, for example at 80 °C, we can distinguish the two slopes for different ranges of deformation rate Fig. 5(a). These different slopes originate from the fact that two separate deformation mechanisms are present, schematically represented in Fig. 5(b). At high temperatures or low strain rates, only the process of crystal slip or intra-lamellar deformation determines the yield stress [54]. At lower temperatures, crystal slip or inter-lamellar deformation starts to actively contribute to the observed yield stresses [55].

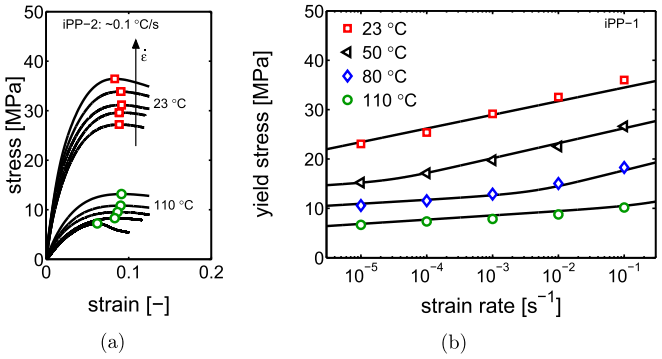

Fig. 4. a) The stress strain response of iPP as a function of strain rate and temperature, and b) The yield kinetics of iPP.

Since the deformation processes act in parallel (stress additive), the observed kinetics can be described by taking the sum of the two separate processes. In this work this is done with the modified Ree-Eyring equation:

$$\sigma_{total} = \sum_{i=I,II} \sigma_i = \sum_{i=I,II} \frac{kT}{V_i^*} sinh^{-1}\left(\frac{\dot{\varepsilon}}{\dot{\varepsilon}_{0,i} exp(-\Delta U_i/kT)}\right) \tag{30}$$

In this equation k is the Boltzman constant, T is the temperature in [K], $\dot{\varepsilon}$ is the applied strain rate, V_i^* is the activation volume of deformation mechanism i, ΔU_i is the activation energy of mechanism i and $\dot{\varepsilon}_{0,i}$ is the rate constant. The temperature and strain rate are specified in the experimental section.

5.3.2. The effect of processing

When we restrict ourselves to the influence of the cooling history a decrease in crystallinity and lamellar thickness is found upon increasing cooling rates. The effect of these structural features on the mechanical properties and in particular the yield stress was

Table 3
Model parameters.

Parameter	iPP-1	iPP-2	Unit
N_{ref}	$2.7\cdot10^{14}$	$1.2\cdot10^{14}$	[m^{-3}]
T_{Nref}	383	383	[K]
c_n	0.181	0.219	[K^{-1}]
G^0_{max}	$4.5\cdot10^{-6}$	$4.81\cdot10^{-6}$	[ms^{-1}]
T^0_{Gref}	363	363	[K]
c_g	$2.3\cdot10^{-3}$	$2.3\cdot10^{-3}$	[K^{-2}]
a	$1.60\cdot10^{-9}$	$1.60\cdot10^{-9}$	[Pa^{-1}]
b	0	0	[Pa^{-2}]
ζ	0.0275	0.0275	[bar^{-1}]

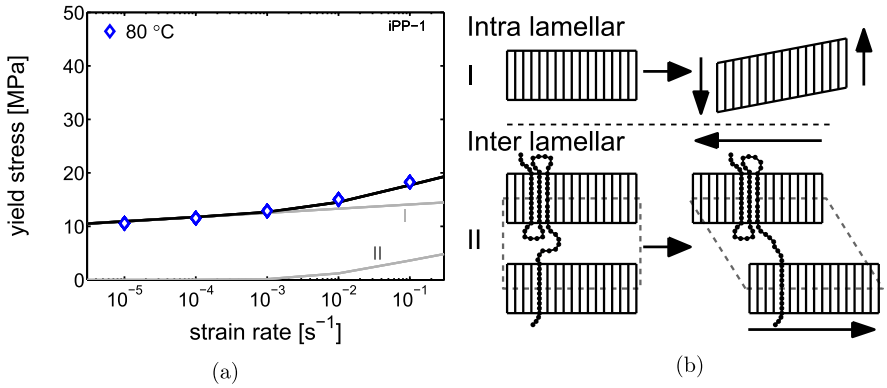

Fig. 5. a): Yield data measured on iPP-1 at a temperature of 80 °C. Two slopes corresponding to separate deformation mechanisms are indicated with I and II. b) Schematic representation of the intra- and interlamellar deformation mechanism.

investigated in Ref. [3], and it was found that the resistance against yield becomes stronger with lower cooling rates. Furthermore it was found that the activation volume and energy in the Ree-Eyring equation are independent of cooling rate, *alpha* nucleating agent or copolymer content. Moreover, the yield kinetics of multiple iPP grades including the ones used in this study, could be described perfectly with the same parameters. The only processing dependent variables in non-isothermal quiescent conditions were found to be the rate constants. Values for V_i^* and ΔU_i are taken from van Erp et al. [3], and listed in Table 4.

5.3.3. Relation between structural features and yield kinetics

The only remaining Eyring parameters to be identified are the rate constants $\dot{\varepsilon}_{0,i}$. The results of van Erp et al. [3] can straightforwardly be translated to obtain the relation between the logarithm of the rate constant and the lamellar thickness, shown in Fig. 6.

The relations associated to the lines depicted in Fig. 6 are given by:

$$\begin{aligned} log(\dot{\varepsilon}_{0,I}) &= -1.90\frac{l_c}{l_{c0}} + 74.01 \\ log(\dot{\varepsilon}_{0,II}) &= -0.76\frac{l_c}{l_{c0}} + 28.12 \end{aligned} \tag{31}$$

with $l_{c0} = 1$ nm. Making use of this empirical relation, which holds for multiple iPP-grades enables us to predict yield kinetics once the lamellar thickness is known. Although the amount of imperfections present within the crystalline domains is cooling rate dependent, a relation between lamellar thickness and rate constant is sufficient to describe the data measured by van Erp et al. [3] under the processing conditions applied in his work.

5.4. The relation between crystallization temperature and lamellar thickness

The lamellar thickness of crystals that grow at a certain temperature T_c is inversely proportional to the undercooling according to [26]

Table 4
List of parameter values.

	V_i^* [nm^3]	ΔU_i [kJ mol^{-1}]
Mechanism *I*	14.20	503.7
Mechanism *II*	4.44	158.0

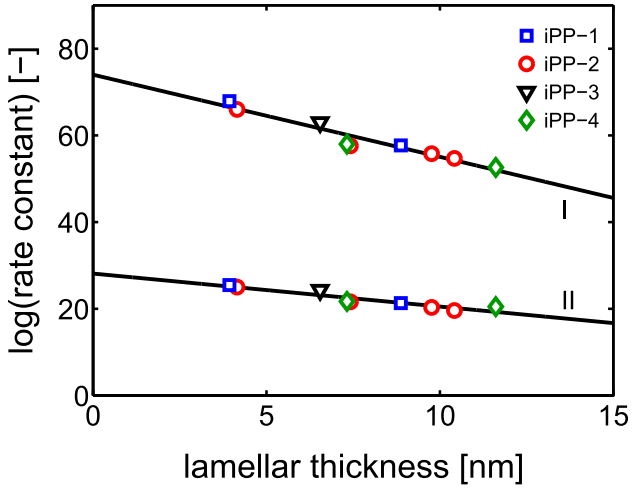

Fig. 6. The relation between lamellar thickness and the rate constants, deduced from Ref. [3].

$$l_c = \frac{2\sigma_e T_m^0}{\Delta h_f \left(T_m^0 - T_c\right)} + \delta l, \tag{32}$$

where σ_e is the surface free energy, Δh_f is the enthalpy of fusion and T_c is the crystallization temperature. T_m^0 is the equilibrium melting temperature, i.e. the melting temperature of a crystal with extremely large lamellar thickness. Here, the equilibrium crystallization temperature is not made pressure dependent since the pressures during the crystallization process are not far from atmospheric pressure as a result of shrinkage due to crystal formation. This first term in Eq. (32) represents a stable condition where the increasing surface energy $2\sigma_e$ equals the reduction in free energy obtained [56]. It should be emphasized that l_c is the lamellar thickness prior to thickening. The last term in Eq. (32), δl, is related to the tendency of the polymer to maximize the crystal growth and basically is a quantity arising from the kinetic nature of crystal growth, given by Ref. [26]:

$$\delta l = \frac{kT_c}{2b_0\sigma}\left[\frac{a_0\Delta h_f \Delta T + 4\sigma T_c^0}{a_0\Delta h_f \Delta T + 2\sigma T_c^0}\right] \tag{33}$$

where k is the Boltzman constant, σ is the lateral surface free energy, b_0 is the thickness of the surface layer and a_0 is the width of

the molecule. At low and moderate cooling rates δ may be approximated by Ref. [57]:

$$\delta l \cong \frac{kT_c}{b_0\sigma} \tag{34}$$

The relation between lamellar thickness and crystallization temperature has been subject of many studies in the past, and an overview of some of these results is given in Fig. 7. For example, Cheng et al. examined iPP with different degrees of stereo defects but similar molecular weight, and determined the lamellar thickness for samples crystallized isothermally at different temperatures [47]. The conclusion that can be drawn from these results is that a unique relation between T_c and l_c exists, independent of the degree of stereo defects. Iijima et al. used two iPP grades with similar isotacticity, but different molecular weights [58]. They found a relationship T_c versus l_c that holds for both their isotactic polypropylenes, independent of molecular weight. On the other hand, Lu et al. [48] used two isotactic polypropylenes with a much bigger difference in molecular weight. They found that as a result of increasing molecular weights, the surface free energy σ_e increases, and thus a shift in T_c versus l_c. This was interpreted as that for the lower molecular weight samples a relatively high amount of extended-chain crystallites are formed, whereas in case of higher molecular weight samples folded chain configurations are preferable. Experiments of Devoy et al. support this interpretation [59]. The T_m^0 on the other hand was found to be unaffected, which is different from what Yamada et al. [60] found in their study. Lu et al. could reasonably resolve this latter disagreement by a crystallization theory proposed by Strobl [61] where the crystallization and melting are non-reversible processes. Based on the findings presented above the important conclusion is drawn that due to different molecular features present in specific iPP grades, deviations in the relation between crystallization temperature and lamellar thickness are found. Therefore this relation is determined for the iPP grades used in this study. The assumption is made that the only variable parameter in Eq. (32) is the surface free energy σ_e. In agreement with Angelloz et al. [23] and Iijima et al. [58] the equilibrium melting temperature T_m^0 is chosen at 193 °C, and used to describe the experimental data sets shown in Fig. 7. An important note that should be emphasized is that the values found for lamellar thickness from X-ray experiments (partly) depend on the techniques used [41]. The interface distribution function as for example used by Iijima et al. gives the most probable value for the lamellar thickness, whereas the correlation function as for example used by Cheng et al. gives the mean value. Finally the relation of T_c versus l_c can be determined with DSC as well, as demonstrated by for example Wlochowicz et al. [62]. Another important note is that in case of extremely narrow molecular weight distributions trends will most likely be different, and only using σ_e to fit the relation is insufficient. The data found for the iPP grades in this work will be described using the same set of parameters, adopted from Xu et al. [63], and are given in Table 5.

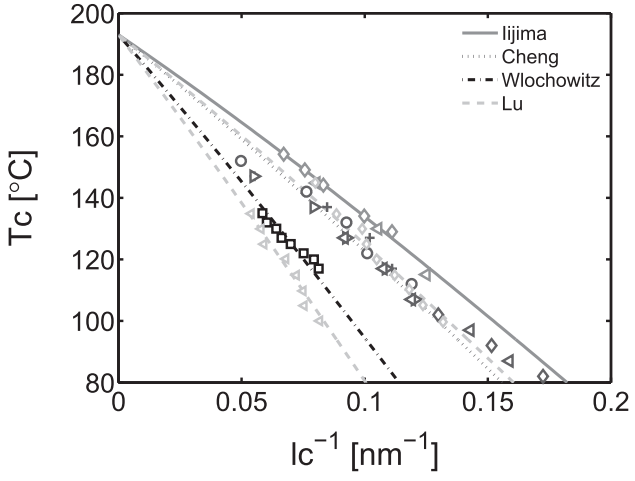

Fig. 7. The relation between lamellar thickness and crystallization temperature. Lines are fitted using an equilibrium melting temperature of 193 °C. Data are reproduced from Refs. [47,58,48,62].

In Fig. 7 it can be seen that experimental data of several authors can be described using this set of parameters, and only varying the value of the surface free energy σ_e. In Table 6 the values of this parameter are given.

The relation between T_c and l_c is determined for isothermal crystallization. For the non-isothermal experiments the temperature-time profiles are divided into discrete temperature steps and for each time step Δt a crystal volume:

$$\Delta V = \Delta t \cdot \dot{\xi} \tag{35}$$

is formed with an associated lamellar thickness obtained from Eq. (32). The additional space filling $\dot{\xi}$, achieved during that specific time step follows from Eq. (29). As a result of the non-isothermal crystallization we predict lamellar thickness distributions.

6. Results and discussion

6.1. Temperature predictions

Crystallization from the melt begins with the formation of point-like nuclei that subsequently grow into spherulites. Due to the kinetics of the crystallization process different morphologies will arise when cooling rates are varied. In this study this was achieved by adjusting the temperature of the cold press, ranging from 20 °C to 90 °C. These temperatures act as boundary conditions in the thermal analysis. The melt was cooled from 220 °C before it was placed in the cold press. In Fig. 8(a) a calculated cooling history of a 1 mm thick sheet in a 20 °C cold press is shown, as a function of time and position. The cooling rates are the highest close to the wall and the lowest in the center. The effect of the latent heat release can be recognised in the center since the decrease in temperature is followed by an increase. Subsequently the temperature decreases again.

To validate the predicted temperature profiles, in-situ time-temperature measurements were performed in case of the slowest and the fastest cooling rates assessed in this work. The small thermocouple with a thickness of approximately 0.4 mm was embedded in the polymer material to record the temperature. Since the thermocouple is relatively thick compared to the polymer sheet, an average temperature over the sheet thickness is measured and, therefore, a comparison is made with the calculated average time-temperature profile, shown in Fig. 8(b). The position of the latent heat release contributions, featured by a plateau in the time-temperature profile, reveal that the crystallization temperatures

Table 5
Model parameters.

Parameter	Value
σ_e [J nm^{-2}]	$146 \cdot 10^{-21}$
T_m^o [K]	466
Δh_f [J nm^{-3}]	$207 \cdot 938 \cdot 10^{-24}$
b_0 [nm]	0.626
σ [J nm^{-2}]	$11.95 \cdot 10^{-21}$

Table 6
Surface free energy.

Author	σ_e[J nm^{-2}]
Iijima	$113.88 \cdot 10^{-21}$
Lu (Mn = 12 kg/mol)	$131.40 \cdot 10^{-21}$
Cheng	$135.78 \cdot 10^{-21}$
Wlochowitz	$191.26 \cdot 10^{-21}$
Lu (Mn = 340 kg/mol)	$219.00 \cdot 10^{-21}$

as expected, the characteristic β and γ peak are negligible with respect to the α peak present at a scattering angle of $2\theta \cong 12.5^o$. Similar results are found for iPP-2.

From Bragg's law the long spacing is obtained and via Eq. (5) this gives the lamellar thickness. The SAXS data of the isothermal experiments, Fig. 9(b), is also used to determine the interface distribution function. The corrections are explained in Section 2.3, and a corrected 1D intensity pattern is visualised in Fig. 10(a). Also the

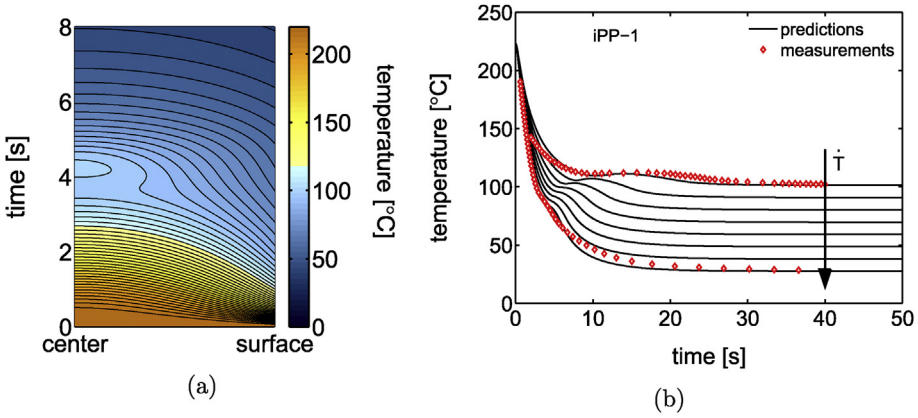

Fig. 8. An example of the predicted temperature profile as a function of time and position. iPP-1 with the cold press set at 20 °C (left) and the average time-temperature history of iPP-1 samples prepared with different cold press temperatures.

decrease with increasing cooling rates. Moreover, it can be seen that the predictions are in good agreement with the experimental results, and that discrepancies arise mainly after the solidification. This can be explained by an increasing thermal contact resistance in the experiments, which is not included in the model. After solidification the material shrinks and as a result the contact pressure reduces. Therefore, the predicted cooling rate is higher than the measured temperature decrease after crystallization.

6.2. X-ray analysis

It is assumed that, under the moderate cooling conditions applied here, only monoclinic alpha phase will be formed and that, therefore, the crystallization model could be simplified to the form presented in Section 5.2. To justify this assumption the wide angle X-ray patterns measured on iPP-1 for all eight cooling rates are depicted in Fig. 9(a). The crystallinities were al within 64± 5% and, interference function is depicted in Fig. 10(a) and is used to calculate the interface distance distribution function using Eq. (8). A typical result is shown in Fig. 10(b) where the IDF of iPP-1 measured at 120 °C is shown. Gaussians are used for deconvolution purposes. First, the most probable long spacing which is corresponding to the first minimum in $g_1(r)$, is fixed. Then, by using the crystallinity obtained via WAXD, ± 5% the ratio between the most probable lamellar thickness and amorphous layer thickness is determined and Gaussians are fitted to obtain the thickness distributions of both the crystalline and amorphous domains. The first maximum in $g_1(r)$ corresponds to α cross hatched structures and is fitted on the resulting part of the IDF [64]. The Gaussian distributions found via this deconvolution procedure are plotted in Fig. 10(b) as well.

An important observation is that, although the quasi-isothermal crystallization would result in nearly uniform lamellar thickness according to Eq. (32), we find distributions. The full width half maximum (FWHM) of the Gaussians is on average 3.25 for the

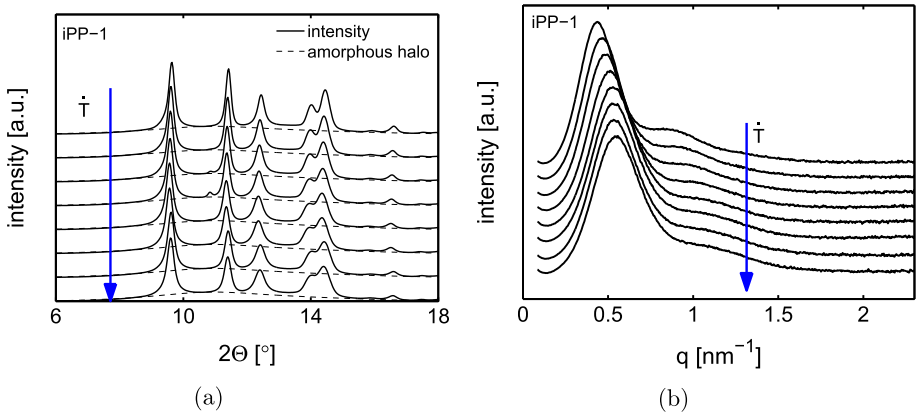

Fig. 9. WAXD patterns (left) and SAXS patterns (right) measured on iPP-1 prepared with different cooling rates by adjusting the cold press temperature.

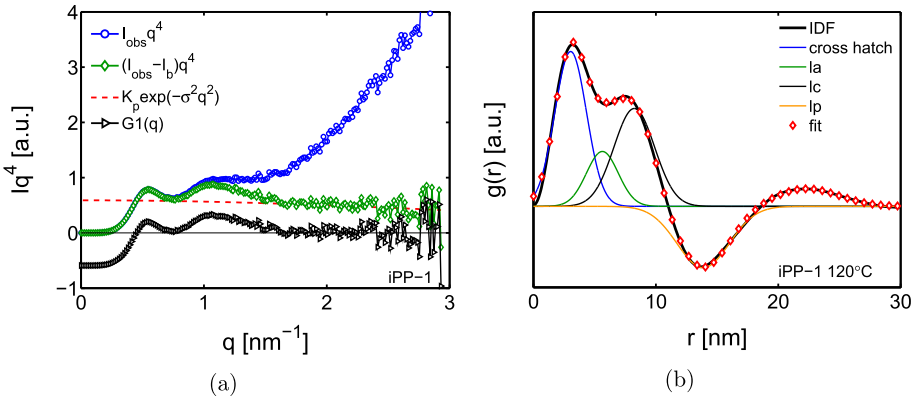

Fig. 10. Correction of the observed intensity for electron density fluctuations and diffuse phase boundaries (left) and an interface distance distribution function obtained from a quasi-isothermal crystallization experiment on iPP-1. The Gaussians obtained from deconvolution indicate the cross-hatch distance distribution (line), the amorphous layer thickness distribution (dashed line), the lamellar thickness distribution (dots) and the long period distribution (dash-dotted).

isothermal crystallization experiments conducted on the two iPP-grades. Consequently, this lamellar thickness distribution is also included in the predictions. At every time step and corresponding crystallization temperature step, a lamellar thickness distribution is formed with this FWHM. In this work the lamellar thickness obtained from the IDF was used since it gives the most probable value for the lamellar thickness [41]. Additionally, the lamellar thickness obtained from the combination of SAXS and WAXD experiments Eq. (5) provides an estimation of the error made using the latter approach. The results are shown in Fig. 11 and they are used in the following part by changing the parameters in Eq. (31) into the corrected ones given by:

$$\begin{aligned} log(\dot{\varepsilon}_{0,I}) &= -2.72\frac{l_{c,IDF}}{l_{c0}} + 78.88 \\ log(\dot{\varepsilon}_{0,II}) &= -1.09\frac{l_{c,IDF}}{l_{c0}} + 30.09 \end{aligned} \tag{36}$$

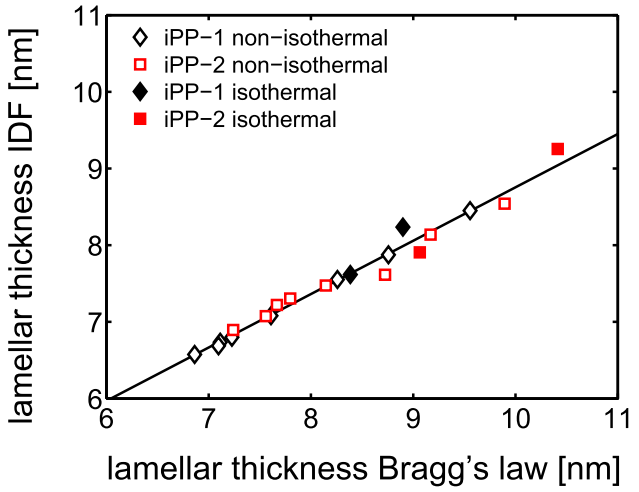

Fig. 11. The lamellar thickness obtained from the interface distance distribution function (IDF) as a function of the lamellar thickness obtained from Bragg's law. Filled markers are from isothermal crystallization experiments and open markers are obtained from non-isothermal crystallization experiments.

6.3. Relation between Tc and lc

As explained in 3.4 experimental data of several authors could be described using Eq. (32) with an equilibrium crystallization temperature of 193 °C and a variable surface free energy. Although different experimental methods for lamellar thickness determination yield differences in the values found, all presented data on the relation between crystallization temperature and lamellar thickness can be described accurately well using the parameters given in Table 5 and a specific value for σ_e for each data set. To obtain the σ_e values for the two iPP-grades used in this study, quasi-isothermal cooling experiments were conducted. In-situ temperature measurements demonstrate that the crystallization took place at conditions close to isothermal, see Fig. 12(a). These temperatures were plotted as a function of the lamellar thickness obtained from the IDF.

From Fig. 12(b) it can be seen that using a surface free energy which is higher for the iPP with the highest molecular weight (iPP-2, $\sigma_e = 155.5 \cdot 10^{-21}$) and lower for the one with the low molecular weight (iPP-1, $\sigma_e = 134.3 \cdot 10^{-21}$) gives good descriptions for the lamellar thickness as a function of the crystallization temperature. Although the value of σ_e is determined on a small number of experimental data points, it seems reasonable with respect to the data reported by other authors. This fits the expectations based on Lu et al. [48], eventhough the differences in molecular weight are so small that it is highly unlikely that this is the only molecular feature causing this difference. From the time-temperature history within the polymer sheet, combined with Eq. (32) and the FWHM of 3.25, the lamellar thickness can be calculated. Summation of the distributions obtained at the different increments during the non-isothermal crystallization process gives the lamellar thickness distribution as a function of the position within the polymer sheet. In Fig. 13(a) an example of such a calculated lamellar thickness distribution profile is shown. In the center where the cooling rate was the lowest, the formed lamellae have the largest average thickness. Furthermore it can be seen that the width of the distribution is similar, independent of the position with respect to the walls of the compression molding machine. Typically the non-isothermal history adds 0.04 to the FWHM of the lamellar thickness distribution. To compare the predicted average lamellar thickness distributions with the experimentally obtained ones, they are plotted in Fig. 13(b) for the different cooling rates. The agreement between predictions and experiments is good for both grades (only results for iPP-1 are shown). The most probable lamellar thickness, as well as the corresponding width of the

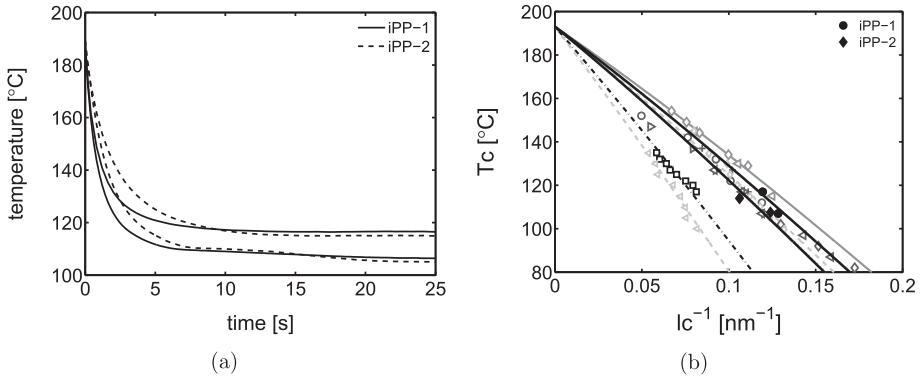

Fig. 12. Temperature measurements in isothermal crystallization experiments (left), and the relation between the lamellar thickness and the crystallization temperature (right). Markers represent experimental data and lines are best fits. Filled markers are obtained from the isothermal experiments conducted on iPP-1 and iPP-2.

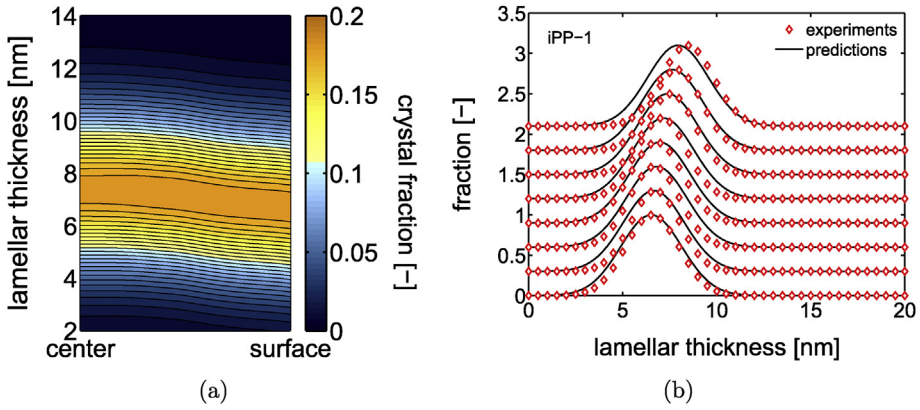

Fig. 13. Predictions of the lamellar thickness distribution as a function of the position with respect to the walls of the mold in an iPP-1 sheet, cooled in a cold press set at 20 °C (left). Predicted (lines) and measured (markers) average lamellar thickness distributions for different cooling rates.

distributions fit the experimental data quite well, and differences of the average l_c are within 5%.

6.4. Yield stress predictions

The lamellar thickness distributions obtained are used to predict the yield stress. Either the average lamellar thickness, or the lamellar thickness distribution can be used as an input for the relation between lamellar thickness and rate constant, see Eq. (31). When lamellae of all thicknesses contribute equally to the resistance against yielding there is actually no difference between the two procedures. To validate the yield stress predictions, experiments at room temperature and at 80 °C at a strain rate of 10^{-3} s^{-1} are carried out. At room temperature, both deformation mechanisms contribute to the yield stress whereas at 80 °C only the contribution of the intra lamellar deformation process contributes to the yield stress. In Fig. 14 it is shown that quantitative agreement is found for both mold temperatures. The differences in yield stress that can be seen between the two grades are in quantitative agreement with the predictions.

Although the two iPP grades used in this study are relatively similar in terms of molecular weight and polydispersity some clear differences can be observed in the level of the yield stress. These differences are first of all reflected in the crystallization model. The nucleation density as a function of temperature and pressure is different for the two grades and can be expected to be unique for every material. The maximum growth rate of the alpha crystals is slightly different for the two materials and as a result of these differences in the crystallization kinetics the range of crystallization temperatures in a non-isothermal cooling process is different. To relate crystallization kinetics and accompanying crystallization temperature to the formation of structural features like, in this case, the lamellar thickness, a material specific relation between these quantities had to be determined. In this work the inequalities were attributed to the differences in molecular chain architecture, and captured by varying the value for the surface free energy σ_e. The relation between lamellar thickness and yield stress contains the same parameters for both the materials, except for the rate constant which follows directly from the average lamellar thickness.

7. Conclusion

The 1D heat balance was successfully combined with a crystallization model capable of predicting the kinetics in non-isothermal pressure dependent quiescent conditions, and enabled us to predict the time-temperature history of two different iPP-grades cooled in a compression molding machine at different rates. Besides the nucleation density as a function of temperature and the maximum growth rate of the α crystals all parameters in the crystallization model were the same for the two grades used in this work. The temperature predictions were experimentally validated using in-situ temperature measurements. The amount of crystal volume as a function of time and temperature followed from the model framework as well, and was used in combination with the Lauritzen Hoffman equation to predict the lamellar thickness distributions formed during the different cooling histories. By only varying the

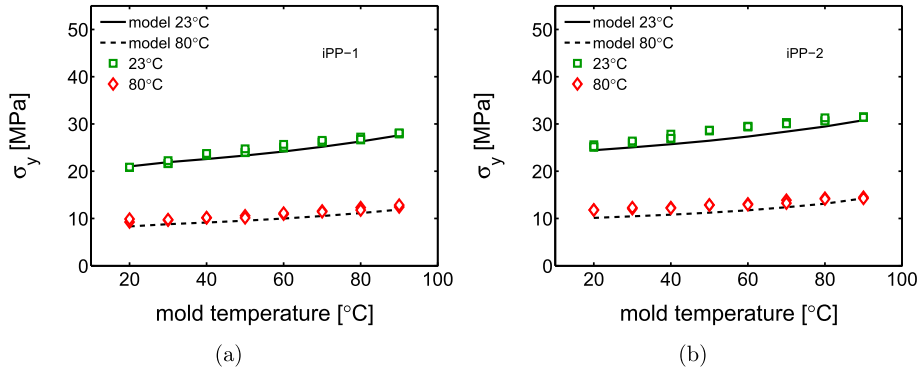

Fig. 14. Yield stress of iPP-1 (left) and iPP-2 (right) at a strain rate of 10^{-3} and temperatures of 23 °C and 80 °C. Lines are model predictions and markers are experimentally obtained data.

surface free energy, which is known to be molecular weight dependent, experimentally obtained data from multiple authors could be described. Therefore it was chosen to find a description of the lamellar thickness as a function of the crystallization temperature by fitting the surface free energy on data measured in-situ during an isothermal crystallization experiment. From this relation lamellar thickness distributions were predicted that were experimentally validated using the interface distribution function. Good agreement was found for both the iPP grades, not only in terms of the average lamellar thickness, but also in terms of the FWHM of the distribution. This confirms that under the cooling conditions applied in this study the Lauritzen-Hoffman equation can be used, despite the absence of isothermal conditions in time and position. Finally, the lamellar thickness distributions were used together with a corrected empirical relation between lamellar thickness and rate constant reported in the work of van Erp et al., Eq. (36). This enabled us to predict the yield stress directly after processing at all loading conditions, i.e. strain rate and temperature. Predictions were made for a strain rate of 10^{-3} and temperatures of 23 °C and 80 °C tensile tests were carried out for validation and the predicted yield stresses of both the iPP grades showed good agreement with the experimentally obtained data at all loading conditions. This work shows that making the connection between processing and mechanical properties is feasible. Extension to flow and multiple crystallographic structures is part of future work.

Acknowledgments

The authors would like to thank the staff at beamline BM26 of the ESRF in France for the help during the experiments. Furthermore, G. Portale is acknowledged for the valuable discussions about the data treatment. We thank NWO for granting beamtime to perform these experiments.

References

[1] F. Auriemma, O. Ruiz De Ballesteros, C. De Rosa, C. Invigorito, Tailoring the mechanical properties of isotactic polypropylene by blending samples with different stereoregularity, Macromolecules 44 (15) (2011) 6026–6038.
[2] T.B. Van Erp, C.T. Reynolds, T. Peijs, J.A.W. Van Dommelen, L.E. Govaert, Prediction of yield and long-term failure of oriented polypropylene: kinetics and anisotropy, J. Polym. Sci. Part B Polym. Phys. 47 (20) (2009) 2026–2035.
[3] T.B. Van Erp, D. Cavallo, G.W.M. Peters, L.E. Govaert, Rate-, temperature-, and structure-dependent yield kinetics of isotactic polypropylene, J. Polym. Sci. Part B Polym. Phys. 50 (20) (2012) 1438–1451.
[4] T.B. Van Erp, L.E. Govaert, G.W.M. Peters, Mechanical performance of injection-molded poly(propylene): characterization and modeling, Macromol. Mater. Eng. 298 (3) (2013) 348–358.
[5] J.J. Janimak, G.C. Stevens, Inter-relationships between tie-molecule concentrations, molecular characteristics and mechanical properties in metallocene catalysed medium density polyethylenes, J. Mater. Sci. 36 (8) (2001) 1879–1884.
[6] A. Lustiger, R.L. Markham, Importance of tie molecules in preventing polyethylene fracture under long-term loading conditions, Polymer 24 (12) (1983) 1647–1654.
[7] J.C. Halpin, J.L. Kardos, Moduli of crystalline polymers employing composite theory, J. Appl. Phys. 43 (5) (1972) 2235–2241.
[8] M. Elmajdoubi, T. Vu-Khanh, Effect of cooling rate on fracture behavior of polypropylene, Theor. Appl. Fract. Mech. 39 (2) (2003) 117–126.
[9] B.A.G. Schrauwen, R.P.M. Janssen, L.E. Govaert, H.E.H. Meijer, Intrinsic deformation behavior of semicrystalline polymers, Macromolecules 37 (16) (2004) 6069–6078.
[10] R. Popli, L. Mandelkern, Influence of structural and morphological factors on the mechanical properties of the polyethylenes, J. Polym. Sci. Part B Polym. Phys. 25 (3) (1987) 441–483.
[11] J.M. Peterson, Thermal initiation of screw dislocations in polymer crystal platelets, J. Appl. Phys. 37 (11) (1966) 4047–4050.
[12] R.J. Young, Screw dislocation model for yield in polyethylene, Mater. Forum 11 (1988) 210–216.
[13] N.W.J. Brooks, M. Mukhtar, Temperature and stem length dependence of the yield stress of polyethylene, Polymer 41 (4) (2000) 1475–1480.
[14] T. Kazmierczak, A. Galeski, A.S. Argon, Plastic deformation of polyethylene crystals as a function of crystal thickness and compression rate, Polymer 46 (21) (2005) 8926–8936.
[15] S.V. Meille, D.R. Ferro, S. Brùckner, A.J. Lovinger, F.J. Padden, Structure of β-isotactic polypropylene: a long-standing structural puzzle, Macromolecules 27 (9) (1994) 2615–2622.
[16] B. Lotz, J.C. Wittmann, A.J. Lovinger, Structure and morphology of poly(-propylenes): a molecular analysis, Polymer 37 (22) (1996) 4979–4992.
[17] L.C.E. Struik, The mechanical behaviour and physical ageing of semicrystalline polymers: 2, Polymer 28 (9) (1987) 1534–1542.
[18] P.B. Bowden, R.J. Young, Deformation mechanisms in crystalline polymers, J. Mater. Sci. 9 (12) (1974) 2034–2051.
[19] K. Mezghani, P.J. Phillips, The γ-phase of high molecular weight isotactic polypropylene: iii. the equilibrium melting point and the phase diagram, Polymer 39 (16) (1998) 3735–3744.
[20] E. Lezak, Z. Bartczak, A. Galeski, Plastic deformation behavior of γ-phase isotactic polypropylene in plane-strain compression at room temperature, Polymer 47 (26) (2006) 8562–8574.
[21] E. Lezak, Z. Bartczak, A. Galeski, Plastic deformation of the γ phase in isotactic polypropylene in plane-strain compression, Macromolecules 39 (14) (2006) 4811–4819.
[22] P.C. Roozemond, M. Van Drongelen, Z. Ma, A.B. Spoelstra, D. Hermida-Merino, G.W.M. Peters, Self-regulation in flow-induced structure formation of polypropylene, Macromol. Rapid Commun. 36 (4) (2015) 385–390.
[23] C. Angelloz, R. Fulchiron, A. Douillard, B. Chabert, R. Fillit, A. Vautrin, L. David, Crystallization of isotactic polypropylene under high pressure (γ phase), Macromolecules 33 (11) (2000) 4138–4145.
[24] S. Piccarolo, Morphological changes in isotactic polypropylene as a function of cooling rate, J. Macromol. Sci. – Phys. B31 (4) (1992) 501–511.
[25] M. Van Drongelen, T.B. Van Erp, G.W.M. Peters, Quantification of non-isothermal, multi-phase crystallization of isotactic polypropylene: the influence of cooling rate and pressure, Polymer 53 (21) (2012) 4758–4769.
[26] J.I. Lauritzen Jr., J.D. Hoffman, Extension of theory of growth of chain-folded polymer crystals to large undercoolings, J. Appl. Phys. 44 (10) (1973) 4340–4352.
[27] V. La Carrubba, S. Piccarolo, V. Brucato, Crystallization kinetics of ipp: influence of operating conditions and molecular parameters, J. Appl. Polym. Sci. 104 (2) (2007) 1358–1367.
[28] G. Lamberti, Isotactic polypropylene crystallization: analysis and modeling, Eur. Polym. J. 47 (5) (2011) 1097–1112.
[29] T.B. Van Erp, P.C. Roozemond, G.W.M. Peters, Flow-enhanced crystallization kinetics of ipp during cooling at elevated pressure: characterization,

validation, and development, Macromol. Theory Simul. 22 (5) (2013) 309–318.
[30] F.J.M.F. Custódio, R.J.A. Steenbakkers, P.D. Anderson, G.W.M. Peters, H.E.H. Meijer, Model development and validation of crystallization behavior in injection molding prototype flows, Macromol. Theory Simul. 18 (9) (2009) 469–494.
[31] J.-W. Housmans, M. Gahleitner, G.W.M. Peters, H.E.H. Meijer, Structure-property relations in molded, nucleated isotactic polypropylene, Polymer 50 (10) (2009) 2304–2319.
[32] W. Bras, I.P. Dolbnya, D. Detollenaere, R. Van Tol, M. Malfois, G.N. Greaves, A.J. Ryan, E. Heeley, Recent experiments on a combined small-angle/wide-angle X-ray scattering beam line at the esrf, J. Appl. Crystallogr. 36 (3 I) (2003) 791–794.
[33] M. van Drongelen, P.C. Roozemond, E.M. Troisi, A.K. Doufas, G.W.M. Peters, Characterization of the primary and secondary crystallization kinetics of a linear low-density polyethylene in quiescent- and flow-conditions, Polymer 76 (2015) 254–270.
[34] J.R. Isasi, L. Mandelkern, M.J. Galante, R.G. Alamo, The degree of crystallinity of monoclinic isotactic poly(propylene), J. Polym. Sci. Part B Polym. Phys. 37 (4) (1999) 323–334.
[35] D. Delaunay, P. Le Bot, R. Fulchiron, J.F. Luye, G. Regnier, Nature of contact between polymer and mold in injection molding. part i: influence of a non-perfect thermal contact, Polym. Eng. Sci. 40 (7) (2000) 1682–1691.
[36] G.R. Strobl, M. Schneider, Direct evaluation of the electron density correlation function of partially crystalline polymers, J. Polym. Sci. Part A-2, Polym. Phys. 18 (6) (1980) 1343–1359.
[37] W. Ruland, The evaluation of the small-angle scattering of lamellar two-phase systems by means of interface distribution functions, Colloid Polym. Sci. Kolloid Z. Z. Polym. 255 (5) (1977) 417–427.
[38] N. Stribeck, W. Ruland, Determination of the interface distribution function of lamellar two-phase systems, J. Appl. Crystallogr. 11 (5) (1978) 535–539.
[39] J.T. Koberstein, B. Morra, R.S. Stein, The determination of diffuse-boundary thicknesses of polymers by small-angle X-ray scattering, J. Appl. Crystallogr. 13 (1) (Feb 1980) 34–45.
[40] B.S. Hsiao, R.K. Verma, A novel approach to extract morphological variables in crystalline polymers from time-resolved synchrotron saxs data, J. Synchrotron Radiat. 5 (1) (1998) 23–29.
[41] C. Santa Cruz, N. Stribeck, H.G. Zachmann, F.J. Baltá Calleja, Novel aspects in the structure of poly(ethylene terephthalate) as revealed by means of small-angle X-ray scattering, Macromolecules 24 (22) (1991) 5980–5990.
[42] M. Kristiansen, T. Tervoort, P. Smith, H. Goossens, Mechanical properties of sorbitol-clarified isotactic polypropylene: influence of additive concentration on polymer structure and yield behavior, Macromolecules 38 (25) (2005) 10461–10465.
[43] C.Y. Yue, W.F. Msuya, Changes in yield in polypropylene of different morphology caused by physical ageing, J. Mater. Sci. Lett. 9 (8) (1990) 985–988.
[44] C. Hedesiu, D.E. Demco, R. Kleppinger, G.V. Poel, K. Remerie, V.M. Litvinov, B. Blümich, R. Steenbakkers, Aging effects on the phase composition and chain mobility of isotactic poly(propylene), Macromol. Mater. Eng. 293 (10) (2008) 847–857.
[45] R. Le Goff, G. Poutot, D. Delaunay, R. Fulchiron, E. Koscher, Study and modeling of heat transfer during the solidification of semi-crystalline polymers, Int. J. Heat Mass Transfer 48 (25–26) (2005) 5417–5430.
[46] R.G. Alamo, M.-H. Kim, M.J. Galante, J.R. Isasi, L. Mandelkern, Structural and kinetic factors governing the formation of the γ polymorph of isotactic polypropylene, Macromolecules 32 (12) (1999) 4050–4064.
[47] Stephen Z.D. Cheng, James J. Janimak, Anqiu Zhang, Eric T. Hsieh, Isotacticity effect on crystallization and melting in polypropylene fractions: 1. crystalline structures and thermodynamic property changes, Polymer 32 (4) (1991) 648–655.
[48] Y. Lu, Y. Wang, Z. Jiang, Y. Men, Molecular weight dependency of surface free energy of native and stabilized crystallites in isotactic polypropylene, ACS Macro Lett. 3 (11) (2014) 1101–1105.
[49] A. Gradys, P. Sajkiewicz, A.A. Minakov, S. Adamovsky, C. Schick, T. Hashimoto, K. Saijo, Crystallization of polypropylene at various cooling rates, Mater. Sci. Eng. A 413–414 (2005) 442–446.
[50] A.N. Kolmogoroff, On the statistic theory of metal crystallization (in russian), Izv. Akad. Nauk. SSSR Ser. Math. 1 (1937) 335–339.
[51] M. Avrami, Kinetics of phase change. i: general theory, J. Chem. Phys. 7 (12) (1939) 1103–1112.
[52] M. Avrami, Kinetics of phase change. ii transformation-time relations for random distribution of nuclei, J. Chem. Phys. 8 (2) (1940) 212–224.
[53] W. Schneider, A. Köppel, J. Berger, Non-isothermal crystallization crystallization of polymers, Int. Polym. Process. II (3–4) (1988) 151–154.
[54] A. Sedighiamiri, L.E. Govaert, M.J.W. Kanters, J.A.W. Van Dommelen, Micro-mechanics of semicrystalline polymers: yield kinetics and long-term failure, J. Polym. Sci. Part B Polym. Phys. 50 (24) (2012) 1664–1679.
[55] R.H. Boyd, Relaxation processes in crystalline polymers: molecular interpretation – a review, Polymer 26 (8) (1985) 1123–1133.
[56] D.C. Bassett, On the role of the hexagonal phase in the crystallization of polyethylene, Adv. Polym. Sci. 180 (2005) 1–16.
[57] J.D. Hoffman, R.L. Miller, Kinetics of crystallization from the melt and chain folding in polyethylene fractions revisited: theory and experiment, Polymer 38 (13) (1997) 3151–3212.
[58] M. Iijima, G. Strobl, Isothermal crystallization and melting of isotactic polypropylene analyzed by time- and temperature-dependent small-angle X-ray scattering experiments, Macromolecules 33 (14) (2000) 5204–5214.
[59] C. Devoy, L. Mandelkern, Effect of molecular weight on the radial growth rates of polymer spherulites, J. Polym. Sci. Part A-2 Polym. Phys. 7 (11) (1969) 1883–1894.
[60] K. Yamada, M. Hikosaka, A. Toda, S. Yamazaki, K. Tagashira, Molecular weight dependence of equilibrium melting temperature and lamellar thickening of isotactic polypropylene with high tacticity, J. Macromol. Sci. – Phys. 42 B (3–4 SPEC.) (2003) 733–752.
[61] G. Strobl, Colloquium: laws controlling crystallization and melting in bulk polymers, Rev. Mod. Phys. 81 (3) (2009) 1287–1300.
[62] A. Wlochowicz, M. Eder, Distribution of lamella thicknesses in isothermally crystallized polypropylene and polyethylene by differential scanning calorimetry, Polymer 25 (9) (1984) 1268–1270.
[63] J. Xu, S. Srinivas, H. Marand, P. Agarwal, Equilibrium melting temperature and undercooling dependence of the spherulitic growth rate of isotactic polypropylene, Macromolecules 31 (23) (1998) 8230–8242.
[64] K. Yamada, S. Matsumoto, K. Tagashira, M. Hikosaka, Isotacticity dependence of spherulitic morphology of isotactic polypropylene, Polymer 39 (22) (1998) 5327–5333.